1 Quasi-Elastic Scattering

1.1 Quasi-Elastic Cross Section Measurement

Quasi-elastic scattering, either with neutrinos or with anti-neutrinos, provides the largest single-channel contribution to the total νN event rate in the threshold regime $E_\nu \leq 2$ GeV. For this reason, precise knowledge of the cross section for this reaction, including its energy dependence and its variation with target nuclei, is important to continued progress in current and future neutrino oscillation experiments. The current state of knowledge of the reaction cross section for neutrino and antineutrino beams is indicated by the compilations of previous experimental measurements shown in Figures 1 and 2. Among the results shown there are normalization uncertainties originating with flux uncertainties which are typically 10-20%. It is readily seen in these plots that existing measurements have large errors throughout the E_ν range accessible by MINERνA (Fig. 1, upper plot), and especially in the threshold regime which is crucial to future neutrino oscillation experiments (Fig. 1, lower plot). Figure 2 shows this problematic lack of precision to pervade the anti-neutrino quasi-elastic cross section measurements as well.

The MINERνA experiment will be able to measure these quasi-elastic cross sections with statistical precisions afforded by event sample sizes which will exceed by two orders of magnitude the samples isolated by the previous generation of (mostly) bubble chamber experiments. In addition, for the first time in neutrino scattering experimentation, precision measurements of the form factors of the nucleon for Q^2 greater than 1 GeV^2 will be possible.

The current level of theoretical understanding is indicated by curves from recent calculations of the cross sections, shown superimposed in Figures 1 and 2. Among multiple different considerations which go into realistic calculations, a primary one concerns consistent, up-to-date treatment of the vector and axial vector form factors which characterize the nucleon weak current. Development of realistic cross section calculations has been underway by researchers of MINERνA for some time. Details can be found in papers by H. Budd, A. Bodek, and J. Arrington [2]; recent parameterizations and fits published by these authors are hereafter designated as "BBA-2003" results. The calculated curves in Figs. 1 and 2 are based upon BBA-2003 form factors with the axial mass parameter of the axial form factors set to M_A=1.00 GeV. In Figs. 1 and 2, the solid curves are calculated without nuclear corrections, while the dashed curves include a Fermi gas model. The dotted curves are calculations for target carbon nuclei and include Fermi motion, Pauli blocking, and the effect of nuclear binding on the nucleon form factors as modelled by Tsushima *et al* [33]. The calculated cross sections are seen to be diminished by $\geq$ 10% as result of inclusion of realistic nuclear corrections. The sensitivity of calculations of this kind to the details of the relevant nuclear physics, shows that an understanding of final state nuclear effects is essential to interpretation of quasi-elastic neutrino measurements. As is related elsewhere in this Proposal, MINERνA is a fine-grained tracking calorimeter designed to enable comparison of quasi-elastic

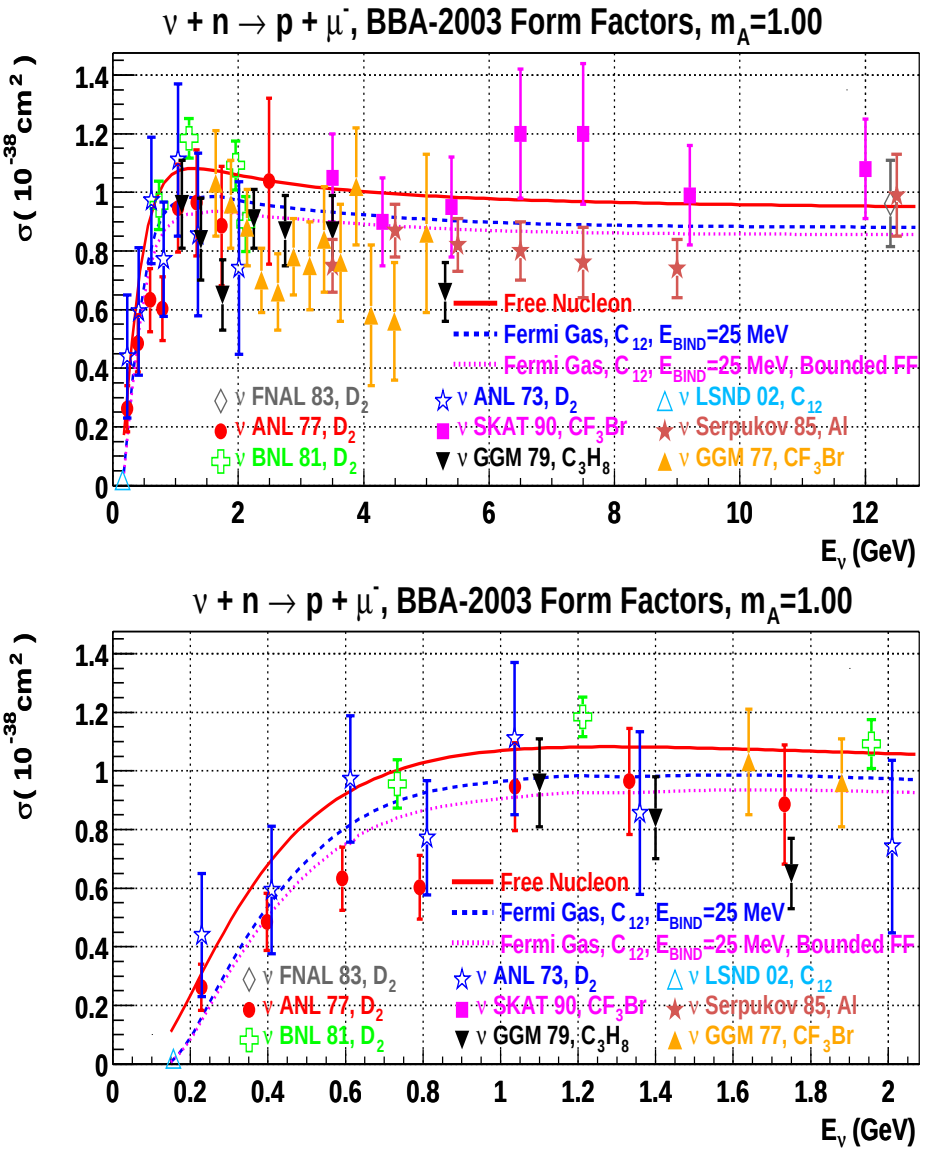

Figure 1: Compilation of experimental measurements of the neutrino quasi-elastic cross section. Existing measurements are characterized by large errors throughout the E_ν range accessible to MINERνA (upper plot), especially so in the crucial threshold regime (lower plot). Representative calculations are shown using BBA-2003 form factors with M_A=1.00 GeV. The solid curve is without nuclear corrections, the dashed curve includes a Fermi gas model [29], and the dotted curve includes Pauli blocking and nuclear binding. The data shown are from FNAL 1983 [17], ANL 1977 [15], BNL 1981 [14], ANL 1973 [22], SKAT 1990 [23], GGM 1979 [24], LSND 2002 [25], Serpukov 1985 [26], and GGM 1977 [27].

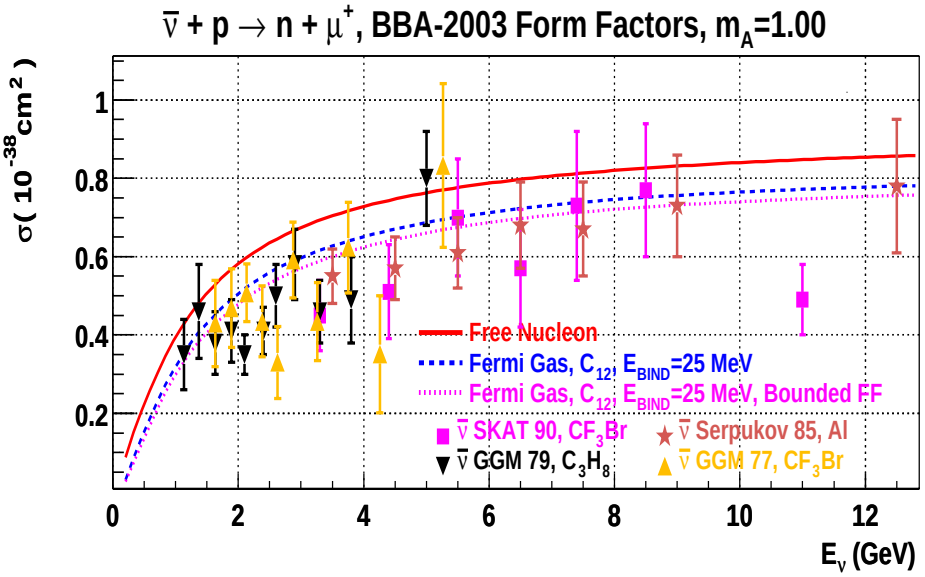

Figure 2: Experimental measurements of the anti-neutrino quasi-elastic cross section over the energy range accessible to MINERνA. As with the neutrino quasi-elastic cross section results of Fig. 1, there is large dispersion among the among the anti-neutrino measurements including systematic differences between individual epxeriments. Theoretical expectations without (solid curve) and including nuclear corrections (dashed, dotted curves) are shown for comparison. The data shown are from SKAT 1990 [23], GGM 1979 [28], Serpukov 1985 [26], and GGM 1977 [27].

(as well as other exclusive channel) production on a variety of target nuclei, consequently knowledge of the contributions from various nuclear target effects can be greatly improved by MINERνA investigations.

1.2 Form Factors of Quasi-Elastic Scattering

The high statistics neutrino quasi-elastic event samples obtainable by MINERνA will enable the Q^2 response of the weak neutral current to be examined with unprecedented accuracy. The underlying V-A structures of the hadronic current include vector and axial vector form factors whose Q^2 response is approximately described by dipole amplitude forms. The essential formalism is given by [3]

$$< p(p_2)|J^+_\lambda|n(p_1) >=$$
$$\overline{u}(p_2)\left[\gamma_\lambda F_V^1(q^2) + \frac{i\sigma_{\lambda\nu}q^\nu\xi F_V^2(q^2)}{2M} + \gamma_\lambda\gamma_5 F_A(q^2) + \frac{q_\lambda\gamma_5 F_P(q^2)}{M}\right]u(p_1),$$

where $q = k_\nu - k_\mu$, $\xi = (\mu_p - 1) - \mu_n$, and $M = (m_p + m_n)/2$. Here, μ_p and μ_n

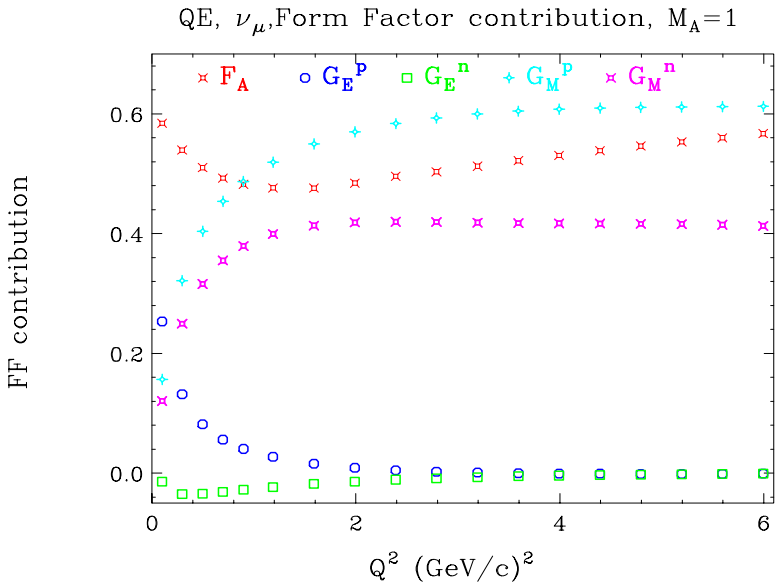

Figure 3: Fractional contributions of G_M^p,G_M^n,G_E^p, G_E^n and F_A to the Q^2 distributions for quasi-elastic neutrino (top) and anti-neutrino (bottom) samples with the NUMI beam configuration.

are the proton and neutron magnetic moments. It is assumed that second-class currents are absent, and so the scalar form-factor F_V^3 and the tensor form-factor F_A^3 do not appear.

The form factors $F_V^1(q^2)$ and $\xi F_V^2(q^2)$ are given by:

$$F_V^1(q^2) = \frac{G_E^V(q^2) - \frac{q^2}{4M^2}G_M^V(q^2)}{1 - \frac{q^2}{4M^2}}, \quad \xi F_V^2(q^2) = \frac{G_M^V(q^2) - G_E^V(q^2)}{1 - \frac{q^2}{4M^2}}.$$

According to CVC, the form factors $G_E^V(q^2)$ and $G_M^V(q^2)$ are directly related to form factors determined via electron scattering $G_E^p(q^2)$, $G_E^n(q^2)$, $G_M^p(q^2)$, and $G_M^n(q^2)$:

$$G_E^V(q^2) = G_E^p(q^2) - G_E^n(q^2), \quad G_M^V(q^2) = G_M^p(q^2) - G_M^n(q^2).$$

The axial form factor F_A and the pseudoscalar form factor F_P (related to F_A by PCAC) are given by

$$F_A(q^2) = \frac{g_A}{\left(1 - \frac{q^2}{M_A^2}\right)^2}, \quad F_P(q^2) = \frac{2M^2 F_A(q^2)}{M_\pi^2 - q^2}.$$

In the quasi-elastic differential cross section, $F_P(q^2)$ is multiplied by $(m_l/M)^2$, consequently its contribution in muon neutrino interactions is very small except

g_A	-1.267
G_F	1.1803×10^{-5} GeV^{-2}
$\cos\theta_c$	0.9740
μ_p	2.793 μ_N
μ_n	-1.913 μ_N
ξ	3.706 μ_N
M_V^2	0.71 GeV^2
M_A	1.00 GeV

Table 1: Values of parameters for the weak nucleon current used in the BBA-2003 calculation of quasi-elastic reaction cross sections.

at very low energy, below 0.2 GeV. In general, the axial form factor $F_A(q^2)$ can only be extracted from quasi-elastic neutrino scattering. At low Q^2 however, the behavior of $F_A(q^2)$ can also be inferred from pion electroproduction data.

Until recently, it has been common practice to assume that form factors are described by the dipole approximation. For example, the vector form factors are often described:

$$G_D(q^2) = \frac{1}{\left(1 - \frac{q^2}{M_V^2}\right)^2}, \quad M_V^2 = 0.71\ GeV^2$$

$$G_E^p = G_D(q^2), \quad G_E^n = 0, \quad G_M^p = \mu_p G_D(q^2), \quad G_M^n = \mu_n G_D(q^2).$$

Note that G_E^p, G_M^p, and G_E^n are positive, while G_M^n and the axial form-factor F_A are negative.

1.3 Axial Form Factor and Axial Mass

Electron scattering experiments continue to provide increasingly detailed determinations of the vector form factors. Neutrino scattering experiments however, are the only plausible route to comparable determinations of the axial form factors, the principal one being the axial form factor $F_A(Q^2)$. The fall-off of the form factor strength with increasing Q^2 is traditionally parameterized using an effective axial vector mass M_A. Its value is known to be $\approx$ 1.00 GeV to an accuracy of perhaps 5%. This value is in agreement with with the theoretically corrected value from pion electroproduction [6], 1.014 ± 0.016 GeV. Uncertainty in the value of M_A contributes directly to uncertainty in the quasi-elastic cross section. Current values of other parameters which enter into calculations (as in BBA-2003) of $\sigma(E_\nu)$ for quasi-elastic reactions, e.g. coupling constants and magnetic moments, are listed in Table 1.

The fractional contributions of F_A and of G_M^p,G_M^n,G_E^p, and G_E^n to the Q^2 distribution for quasi-elastic neutrino and anti-neutrino running with the NUMI beam configuration are shown in Figure 3. The contributions were determined by comparing the cross section calculated using BBA-2003 form-factors and the

cross section with each of the form-factors set to zero. (Because of interference terms, the sum of the fractions does not have to add up to 100%.)

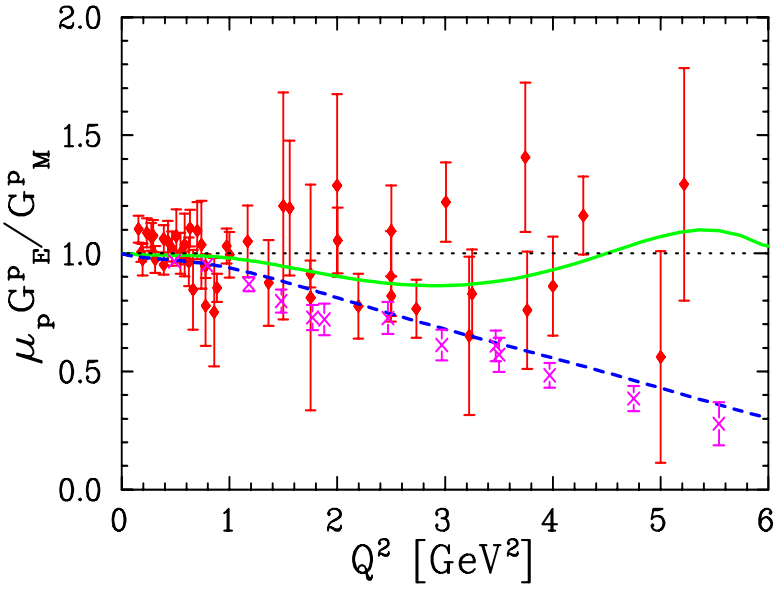

Figure 4: Ratio of G_E^p to G_M^p as extracted by Rosenbluth separation measurements (diamonds) and as obtained by polarization measurements(diamonds). There measurements are seen to be in disagreement at high Q^2; only a small uncertainty however is implied for the neutrino quasi-elastic total cross section.

1.4 Vector Form Factors; Discrepancy at High Q^2

Electron scattering experiments at SLAC and Jefferson Lab (JLab) have measured the vector electromagnetic form factors for the proton and neutron with high precision. The vector form factors can be determined from electron scattering cross sections using the standard Rosenbluth separation technique [7], which is sensitive to radiative corrections, or from polarization measurements using the newer polarization transfer technique [11]. The polarization measurements do not directly measure form factors, but measure the ratio G_E/G_M. These form factors can be related to the vector form factors for quasi-elastic neutrino scattering by the conserved vector current (CVC) hypothesis. Of course, more accurate form factors enable improved calculations for for quasi-elastic neutrino scattering.

Recently however, discrepancies in electron scattering determinations of some vector form factors have appeared, the origins of which may be resolvable by study of quasi-elastic reactions in MINERνA. Figure 4 shows the BBA-2003 fits to $\mu_p\ G_E^p/G_M^p$. There appears a discrepancy between two different methods of measuring the ratio of electric and magnetic form factor for the proton. The fit

including only cross section data (i.e. using Rosenbluth separation) is roughly flat versus Q^2 ($Q^2 = -q^2$) and is consistent with form factor scaling. This is what is expected if the electric charge and magnetization distributions in the proton are the same. However, the new technique of polarization transfer yields a much lower ratio at high Q^2, and indicates a difference between the electric charge and magnetization distributions of the proton. The polarization transfer technique is believed to be more reliable and less sensitive to radiative effects from two-photon corrections.

If the electric charge and magnetization distributions of the proton are indeed very different, a test of the high Q^2 behavior of the axial form factor can provide very useful additional input towards resolving differences among electron scattering measurements. An accurate mapping of axial behavior at high Q^2 can be done in MINERνA.

Current experiments at JLab aim to better understand the source of the disagreement by looking at the recoil proton in elastic electron-proton scattering, thereby minimizing the sensitivity to the dominant sources of uncertainty in previous Rosenbluth separations. Fortunately, since this discrepancy is most prominent at high Q^2, it introduces a relatively small uncertainty to the *total* neutrino quasi-elastic cross section.

1.5 Form Factor Deviations from Dipole Form

Electron scattering results show that dipole amplitudes provide only a first-order description of form factor trends at high Q^2. For example, Figure 5 shows the deviation of G_M^p from dipole-type Q^2 fall-off. In general, the deviations are different for each of the form factors.

In the fits carried out by BBA-2003, the form factors are usually described using an inverse polynomial:

$$G_{E,M}^N(Q^2) = \frac{G_{E,M}^N(Q^2=0)}{1 + a_2 Q^2 + a_4 Q^4 + a_6 Q^6 + ...}.$$

The one exception is for G_E^N, for which a useful parameterization has been given by Krutov *et. al.* [12]:

$$G_E^n(Q^2) = -\mu_n \frac{a\,\tau}{1 + b\tau} G_D(Q^2), \quad \tau = \frac{Q^2}{4M^2},$$

with $a = 0.942$ and $b = 4.61$.

Figure 6 shows the ratio of the predicted neutrino (anti-neutrino) quasi-elastic cross section on nucleons using the BBA-2003 vector form factors compared to the prediction using the dipole vector form factors (with G_E^n=0 and M_A kept fixed). This plot shows that it is important to use most current form factor parameterizations. In MINERνA, it will be possible to test for form factor structures which are more elaborate than simple dipole fall-off with increasing Q^2, the approximation which has been used by all neutrino experiments to date.

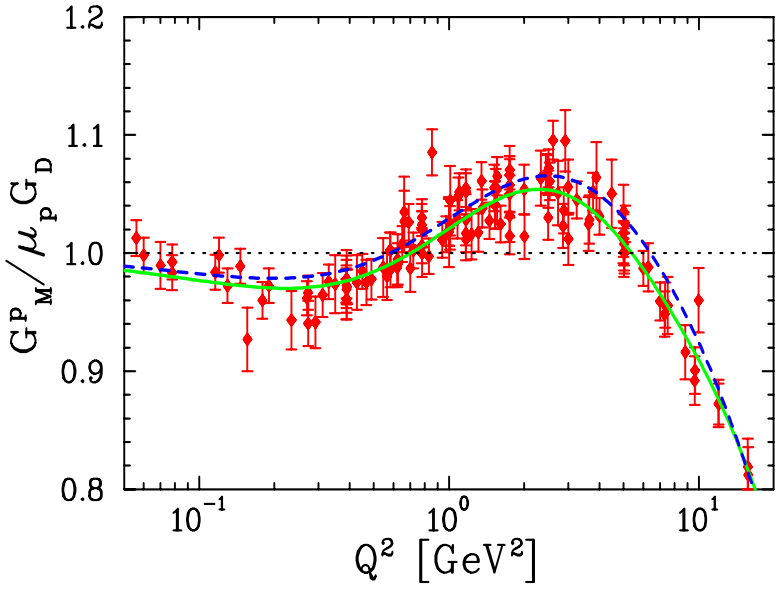

Figure 5: BBA-2003 fits to $G_M^p/\mu_p G_D$. The variation of the ratio from 1.0 indicates deviation from a pure dipole form; the deviation is quite pronounced for Q^2 above 1 GeV^2.

1.6 Nuclear Effects in Quasi-elastic Scattering

There are three important nuclear effects in quasi-elastic scattering from nuclear targets: Fermi motion, Pauli blocking, and corrections to the nucleon form factors due to distortion of the nucleon's size and its pion cloud in the nucleus. Figure 7 shows the nuclear suppression versus Q^2 from a NUANCE [32] calculation [29] using the Smith and Moniz [30] Fermi gas model for carbon. This nuclear model includes Pauli blocking and Fermi motion but not final state interactions. The Fermi gas model was run with a 25 MeV nuclear potential binding energy ϵ and 220 MeV/c Fermi momentum K_f. Figure 8 from Moniz et. al. [30] shows how the effective k_f and nuclear potential binding energy ϵ (within a Fermi-gas model) for various nuclei is inferred from electron scattering data. The effective k_f is extracted from the width of the electron scattered energy, and the nuclear potential binding energy ϵ is extracted from the shifted location of the quasi-elastic peak.

The predicted distortion that nuclear binding exerts on the nucleon form factors in neutrino scattering is indicated in Figure 9. The effect is displayed as ratios of bound to free nucleon form factors for F_1, F_2, and F_A.

Both the Pauli blocking and the nuclear modifications to bound nucleon form-factors reduce the quasi-elastic cross section relative to the cross section with free nucleons. However, it is possible that the low Q^2 deviations are not actual modifications of the nucleon form factors, but rather are effects of inter-

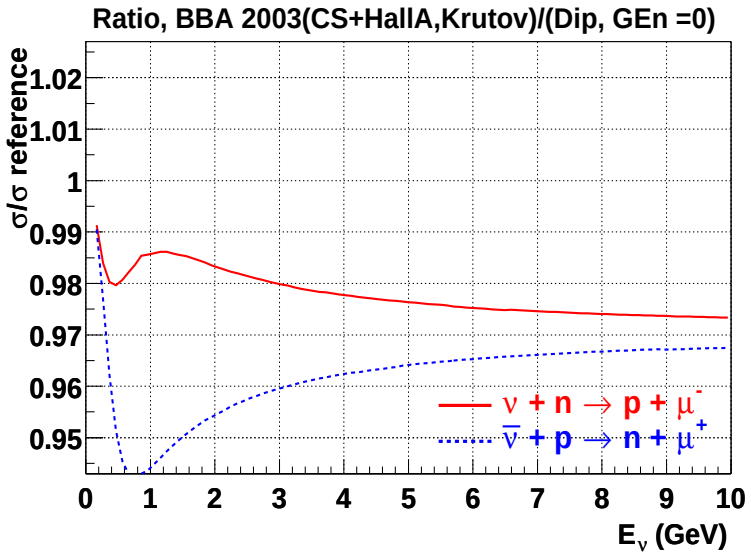

Figure 6: Ratio versus energy of the neutrino (anti-neutrino) quasi-elastic cross section using BBA-2003 form factors, to the expectation using the dipole approximation with G_E^n=0.

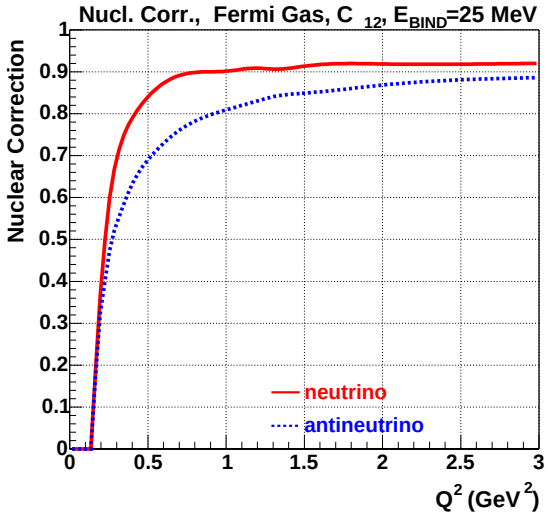

Figure 7: Pauli blocking suppression for a Fermi gas model for carbon with binding energy and Fermi momentum cutoff set to 25 MeV and 220 MeV/c respectively. A suppression of this magnitude is expected for quasi-elastic reactions in MINERνA.

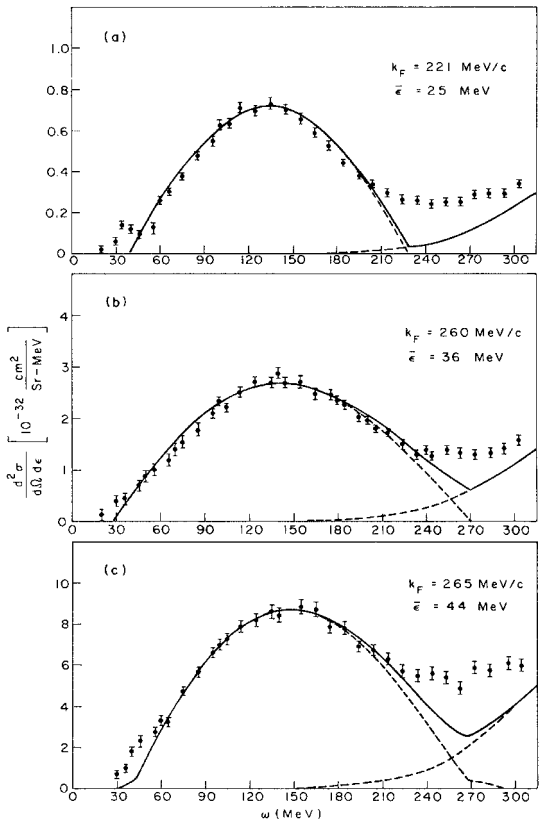

Figure 8: Extraction of Fermi gas model parameters i.e. the effective k_f and nuclear potential binding energy ϵ, from 500 MeV electron scattering data (from Moniz. [30]. Distributions shown represent scattering from (a) carbon, (b) nickel, and (c)lead.

action with the pion cloud for Q^2 less than 1 GeV^2. Note that data from JLab indicate that the binding effects on the form factors should be very small at higher Q^2.

1.7 Detection of Recoil Nucleons

In neutrino experiments, detection of the recoil nucleon is highly useful in distinguishing quasi-elastic from inelastic events. Consequently, knowledge of probabilities for outgoing protons to reinteract with the remaining target nucleons is highly desirable. Similarly, quasi-elastic scattering with nucleons in the high momenta region of the spectral functions needs to be understood. More sophisticated treatments than the simple Fermi Gas model are required. Conversely, inelastic events (such as in resonance production) may be misidentified

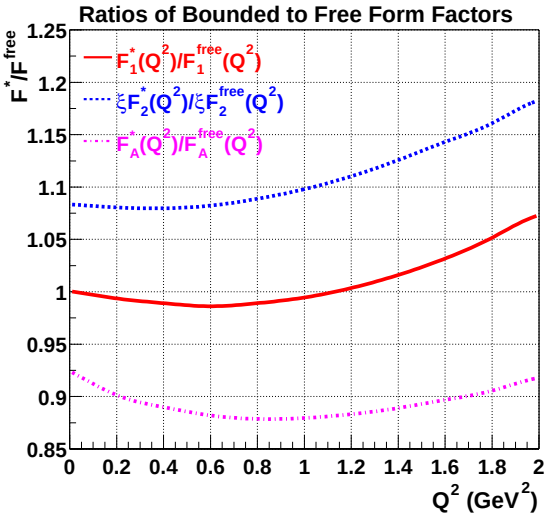

Figure 9: The ratio of bound nucleon (in carbon) to free nucleon form-factors for F_1, F_2, and F_A from ref [33]. Binding effects on the form factors are expected to be very small at higher Q^2 (therefore, this model is not valid for Q^2 greater tha 1 GeV^2

as quasi-elastic events if the final state pion is absorbed in the nucleus. An optimal way to model these effects is to analyze samples of electron scattering data on nuclear targets (including the hadronic final states) and test the effects of the experimental cuts on the final-state nucleons. MINERνA can address the issues arising with proton intranuclear rescattering by investigating nuclear binding effects on neutrino scattering in carbon, and then comparing the data to observations obtained in similar kinematic regions as obtained by electron scattering at JLab. Indeed, MINERνA researchers of the Rochester group will be working with the CLAS collaboration to study hadronic final states in electron scattering on nuclear targets using existing JLab Hall B CLAS data. This analysis will provide information on hadronic final states in quasi-elastic and inelastic resonance production in electron scattering, and will enable the testing of theoretical models to be used in both electron and neutrino experiments. In addition, collaborative work is underway with the Ghent nuclear physics group in Belgium [35], to model both electron and neutrino quasi-elastic scattering on nuclei over the entire range of Q^2. This work will develop the theoretical tools needed to do a precise extraction of the axial form-factor of the nucleon using MINERνA quasi-elastic data on carbon. It is envisaged that nearly identical analyses will be carried out on both neutrino and electron scattering data in the same range of Q^2.

By way of illustration, Figure 10 shows electron scattering data in the quasi-

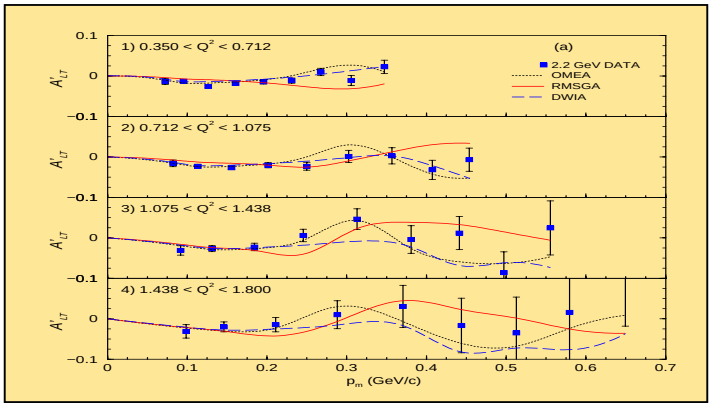

Figure 10: Comparison between $e - e' - P$ electron scattering data on carbon taken with incident electron energy of 2.2. GeV. Here both final-state electron and proton are both detected. Data and two theoretical models are compared as a function of the recoil proton momentum.

elastic region (for carbon) in which the final-state electron and proton are both detected, compared to predictions of theoretical models, as a function of the recoil proton momentum. Extension of the models to neutrino scattering is currently under way.

1.8 Extraction of the Axial Vector Form Factor

Previous neutrino measurements, mostly bubble chamber experiments on deuterium, extracted M_A using the best known assumptions at the time. Changing these assumptions changes the extracted value of M_A. Hence, a prerequisite fo new determinations of M_A is that the most recent form factor parameterizations and couplings be used.

Figure 11 shows the Q^2 distribution from the Baker *et al.* [14] neutrino experiment compared to the prediction assuming dipole form factors with $G_E^n = 0$ and $M_A = 1.100$ GeV. Also shown are the prediction using BBA-2003 form factors and M_A=1.050 GeV. Utilization of more accurate electromagnetic form factors requires a different M_A value in order to describe the same Q^2 distribution. Thus, with the same value of g_A, the use of dipole form factors (and $G_E^n = 0$) instead of the BBA-2003 form factors may lead to an error in extracted value of M_A of 0.050 GeV.

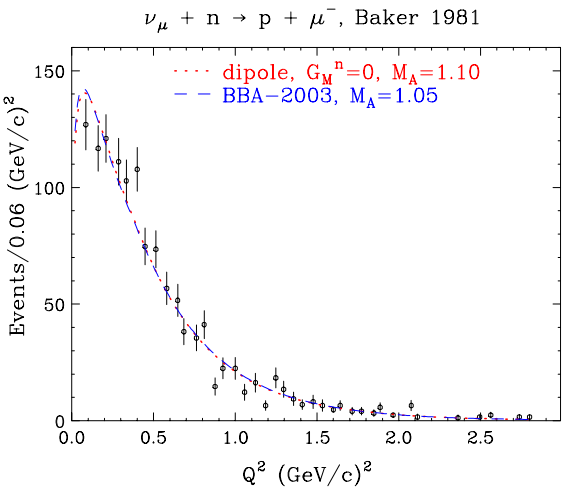

Figure 11: A comparison of the Q^2 distribution using two different sets of form-factors. The data are from Baker *et al.* [14]. The dotted curve uses dipole form factors with $G_E^n = 0$ and $M_A = 1.10\ GeV$. The dashed curve uses the more accurate BBA-2003 form factors and require $M_A = 1.05\ GeV$. It is important to use the most current information on vector form factors from electron scattering experiments when extracting the axial form factor from neutrino data.

1.9 Measurement of the Axial Form Factor in MINERνA

Current and future high-statistics neutrino experiments at low energies (e.g. MiniBooNE, J-PARC and MINERνA) use an active nuclear target such as scintillator (mostly carbon). The maximum Q^2 values that can be reached with incident neutrino energies of 0.5, 1.0, 1.5 and 2 GeV are 0.5, 1.2, 2.1 and 2.9 GeV^2 respectively. Since MiniBooNE and J-PARC energies are in the 0.7 GeV range, these experiments probe the low $Q^2 < 1$ GeV^2 region where nuclear effects are large (see Figures 7 and 9) and where the axial form factor is known rather well from neutrino data on deuterium (see Figure 11). The low Q^2 ($Q^2 < 1$ GeV^2) MiniBooNE and J-PARC experiments can begin to investigate the various nuclear and binding effects in carbon.

At higher Q^2, as shown by the BBA-2003 fits, the dipole approximation can be in error by as much as a factor of two for the vector form factors when $Q^2 > 2$ GeV^2. There is clearly no reason to assume this form will be valid for the axial form factors. As shown in Figure 11 there is very little data for the axial form factor in the high Q^2 region (where nuclear effects are smaller). Both the low Q^2 ($Q^2 < 1$ GeV^2) and high Q^2 ($Q^2 > 2$ GeV^2) regions are accessible in higher energy experiments such as MINERνA which can span the 2-8 GeV energy neutrino range. A MINERνA determination of the axial form factor in the high Q^2 region is of keen interest to on-going investigations of the vector and axial structure of the neutron and proton.

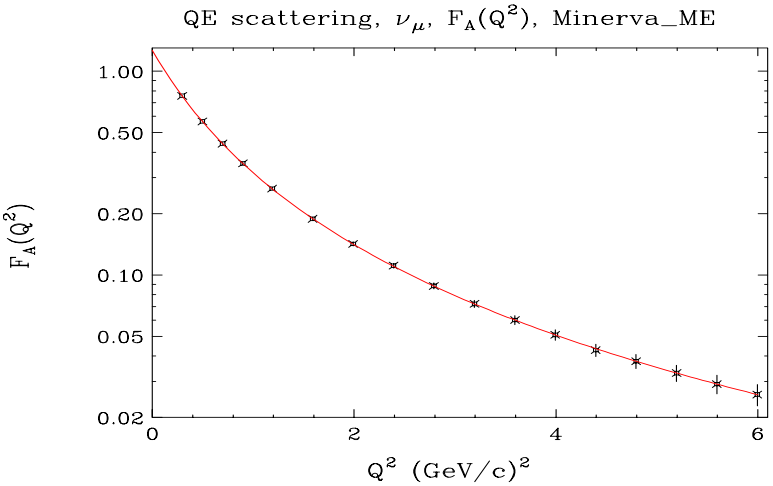

Figure 12: Estimation of values and errors (logarithmic scale) of F_A from a sample of Monte-Carlo neutrino quasi-elastic events recorded in the MINERνA active carbon target. Here, F_A is assumed to be a pure dipole form factor with M_A of 1 GeV. The reaction sample is the estimated yield from four years of NuMI running.

Figure 12 shows the extracted values and errors of F_A in bins of Q^2 from a sample of Monte-Carlo quasi-elastic interactions recorded in the MINERνA active carbon target, from a four-year exposure in the NUMI beam. It can be seen that the high Q^2 regime which is inaccessible to MinibooNE and J-PARC, will be well-resolved in MINERνA.

Figure 13 shows the these results as a ratio of F_A/F_A(Dipole). The lower plot assumes that this ratio is described by the ratio of G_E^p(Cross-Section)/G_E^p(dipole), which was the the accepted result for G_E^p before the new polarization transfer measurement. The upper plot shows a ratio of 1.0 which is expected if the axial form factor is described exactly by the dipole form

References

[1] Y. Fukada *et al.*, Phys. Rev. Lett. 81 (1998) 1562.

[2] H. Budd, A. Bodek and J. Arrington, hep-ex/0308005 (published in Proceedings of NuInt02 - this conference, Nucl, Phys. B, Proceedings Suppl); A. Bodek, H. Budd and J. Arrington, hep-ex/0309024 (to be published in Proceedings of CIPANP2003, New York City, NY 2003.

[3] C.H. Llewellyn Smith, Phys. Rep. 3C (1972).

[4] S. Adler, Phys. Rev. **143**, 1144 (1966); F. Gillman, Phys. Rev. **167**, 1365 (1968).

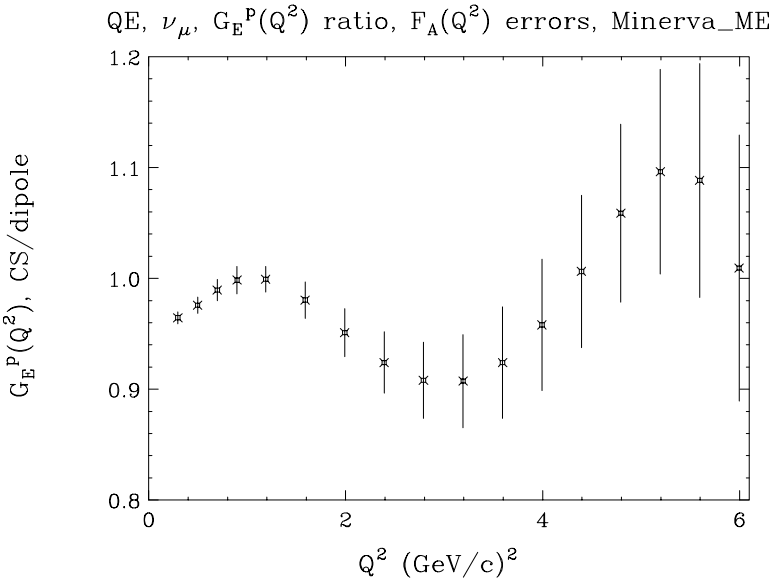

Figure 13: The extracted ratio and error of F_A/F_A(Dipole) from a sample of Monte-Carlo quasi-elastic interactions recorded in the MINERνA active carbon target, from a four-year exposure in the NUMI beam. The lower plot assumes that this ratio is described by the ratio of G_E^p(Cross-Section)$/G_E^p$(dipole), which was the the accepted result for G_E^p before the new polarization transfer measurement. The upper plot shows a ratio of 1.0 which is expected if the axial form factor is described exactly by the dipole form.

[5] D. Drechsel, B. Pasquini, M. Vanderhaeghen, hep-ph/0212123.

[6] V. Bernard, L. Elouadrhiri, U.G. Meissner, J.Phys.G28 (2002), hep-ph/0107088.

[7] J. Arrington, nucl-ex/0305009.

[8] E. J. Brash*et al.*Phys., Rev. C, 65, 051001(R)

[9] M. Paschos, private communication

[10] M. Strikman, private communication. See also talk by Rholf Ent, these proceedings; L. Lapikas, et al Phys.Rev.C61:064325,2000 (nucl-ex/9905009); L. Frankfurt, M. Strikman and M. Zhalov, Phys.Lett.B503:73-80,2001 (hep-ph/0011088).

[11] M. K. Jones *et al.*, Phys. Rev. Lett, 84, (2000) 1398 ; O. Gayou *et al.*, Phys. Rev. Lett, 88 (2002) 092301.

[12] A.F. Krutov, V.E. Troitsky, Eur. Phys. J. A16 (2003) 285, hep-ph/0202183.

[13] S. Glaster *et al.*, Nucl. Phys. B32 (1971) 221.

[14] N.J. Baker *et al.*, Phys. Rev. D23 (1981) 2499.

[15] S.J. Barish *et al.*, Phys. Rev. D16 (1977) 3103.

[16] K.L. Miller *et al.*, Phys. Rev. D26 (1982) 537.

[17] T. Kitagaki *et al.*, Phys. Rev. D26 (1983) 436.

[18] T. Kitagaki *et al.*, Phys. Rev. Lett. 49 (1982) 98.

[19] M.G. Olsson, E.T. Osyporeski and E.H. Monsay, Phys. Rev. D17 (1978) 2938.

[20] S.K. Singh, Nucl. Phys. B36 (1972) 419.

[21] Particle Data Group, Eur. Phys. J C15 (2000) 196.

[22] W.A. Mann *et al.*, Phys. Rev. Lett. 31 (1973) 844.

[23] J. Brunner *et al.*, Z. Phys. C45 (1990) 551.

[24] M. Pohl *et al.*, Lett. Nuovo Cimento 26 (1979) 332.

[25] L.B. Auerbach *et al.*, Phys. Rev. C66 (2002) 015501.

[26] S.V. Belikov *et al.*, Z. Phys. A320 (1985) 625.

[27] S. Bonetti *et al.*, Nuovo Cimento 38 (1977) 260.

[28] N. Armenise *et al.*, Nucl. Phys. B152 (1979) 365.

[29] G. Zeller, private communication.

[30] R.A. Smith and E.J. Moniz, Nucl. Phys. B43 (1972) 605; E. J. Moniz *et al.*, Phys. Rev. Lett. 26. 445 (1971); E. J. Moniz, Phys. Rev. 184, 1154 (1969).

[31] E. J. Moniz, private communication; W. Czyz and K. Gottfried, Nucl. Phys. **21**, 676 (1961); W. Czyz and K. Gottfried, Ann. Phys. NY **21**, 47 (1963);K. Gottfried, *ibid*, **21**, 29 (1963).

[32] D. Casper, Nucl. Phys. Proc. Suppl. 112 (2002) 161.

[33] K. Tsushima, Hungchong Kim, K. Saito, nucl-th[0307013].

[34] A. Bodek and J. L. Ritchie, Phys. Rev. D23 (1981) 1070; ibid Phys. Rev. D24 (1981) 1400.

[35] Ghent Theory group in Belgium (Jan Ryckebusch, jan@inwpent5.UGent.be)

[36] JLab hydrogen experiment 94-110, C.E. Keppel spokesperson.

(http://www.jlab.org/exp_prog/proposals/94/PR94-110.pdf)

[37] JLab deuterium experiment 02-109, C.E. Keppel, M. E. Christy, spokespersons.

(http://www.jlab.org/exp_prog/proposals/02/PR02-109.ps)

.

[38] JLab experiment 99-118 on the nuclear dependence of R at low Q^2, A. Brull, C.E. Keppel spokespersons.

(http://www.jlab.org/exp_prog/proposals/99/PR99-118.pdf)

[39] Jlab Proposal PR03-110 on Nuclear Targets (C, Fe), A. Bodek and C. E. Keppel, Spokespersons; proposed to be run at the same time as deuterium experiment E02-109.

http://www.pas.rochester.edu/~bodek/jlab/Rnuclear-E03-110.pdf